constant, J/mole
$(-\Delta H)$ = heat of reaction, J/mole
h_T = heat transfer coefficient, J/cm^2-s-°C
j_D = j factor for mass transfer
j_H = j factor for heat transfer
k_d^0 = preexponential factor for deactivation, s^{-1}
k_g = mass transfer coefficient, cm/s
M_T = thiophene capacity term, mole/cm^3-cat
N_{Bi_h} = heat Biot number
N_{Bi_m} = mass Biot number
N_{Pr} = Prandtl number
N_{Sc} = Schmidt number
r = radial variable, cm
R_p = particle radius, cm
r_B = rate of reaction of benzene, mole/s-g
r_D, r_T = rate of deactivation or adsorption of thiophene, mole/s-g
s = activity variable in model
S = global activity
t = time, min
T = temperature, °C
ΔT_x = $T_s - T_0$, interphase temperature difference, °C
$(\Sigma|\Delta T|)$ = average temperature deviation function
λ_e = effective thermal conductivity, J/cm-s-°C
ρ = density, g/cm^3
Ω = observed overall rate of reaction, mole/s-g

LITERATURE CITED

Benham, C. B., and V. E. Denny, "Transient Diffusion of Heat, Mass Species, and Momentum in Cylindrical Pellets during Catalytic Oxidation of CO," *Chem. Eng. Sci.*, **27**, 2163 (1972).

Butt, J. B., D. M. Downing, and J. W. Lee, "Inter-Intraphase Temperature Gradients in Fresh and Deactivated Catalyst Particles," *Ind. Eng. Chem. Fundamentals*, **16**, 270 (1977).

Carberry, J. J., "Yield in Chemical Reactor Engineering," *Ind. Eng. Chem.*, **58**, 40 (1966).

———, "On the Relative Importance of External-Internal Temperature Gradients in Heterogeneous Catalysis," *Ind. Eng. Chem. Fundamentals*, **14**, 129 (1975).

Downing, D. M., "Experimental and Modeling Study of the Influence of Deactivation and Catalyst Dilution on a Non-isothermal Catalytic Pellet," Ph.D. dissertation, Northwestern Univ., Evanston, Ill. (1977). Available from University Microfilms.

Kehoe, J. P. G., "The Thermal Response and Kinetic Behavior of a Catalyst Pellet under the Influence of Diffusion," Ph.D. dissertation, Yale Univ., New Haven, Conn. (1971).

———, and J. B. Butt, "Kinetics of Benzene Hydrogenation by Supported Nickel at Low Temperature," *J. Appl. Chem. Biotechnol.*, **22**, 23 (1972*a*).

———, "Interactions of Inter- and Intraphase Gradients in a Diffusion Limited Catalytic Reaction," *AIChE J.*, **18**, 347 (1972*b*).

Koh, H. P., and R. Hughes, "Catalyst Temperature Profiles under Poisoned Conditions," *ibid.*, **20**, 395 (1974).

Lee, J. W., "Effects of Intraparticle Deactivation on Catalyst Performance," Ph.D. dissertation, Northwestern Univ., Evanston, Ill. (1976). Available from University Microfilms.

———, J. B. Butt, and D. M. Downing, "Kinetic, Transport and Deactivation Rate Interactions on Steady State and Transient Responses in Heterogeneous Catalysis," *AIChE J.*, **24**, 212 (1978).

Lee, J. C. M., and D. Luss, "Maximum Temperature Rise Inside Catalytic Pellets," *Ind. Eng. Chem. Fundamentals*, **8**, 596 (1969).

———, "The Effect of Lewis Number on the Stability of a Catalytic Reaction," *AIChE J.*, **16**, 620 (1970).

Prater, C. D., "The Temperature Produced by Heat of Reaction in the Interior of Porous Particles," *Chem. Eng. Sci.*, **8**, 284 (1958).

Wakao, N., and J. M. Smith, "Diffusion in Catalyst Pellets," *ibid.*, **17**, 825 (1962).

Manuscript received June 2, 1978; revision received December 4, and accepted January 11, 1979.

Steady Nonionic Countergradient Transport Through Membranes by Coupled Diffusion

R. H. NOTTER
Y. M. TAM
and
S. MIN

Department of Chemical Engineering
The Pennsylvania State University
University Park, Pennsylvania 16802

Coupled diffusion generated countergradient transport through membranes is analyzed by experimental and theoretical means. Membrane wedge interferometer experiments on an ethanol-water-cellophane membrane system show that net countergradient mass transfer of the less permeable component ethanol may be generated over a wide concentration range. A theoretical analysis of an idealized membrane separating two binary bulk solutions is developed to display further the major features of diffusional coupling effects, and good agreement between observed and predicted countergradient transport characteristics is shown.

SCOPE

A new technique for the study of steady state one-dimensional membrane transport has recently been presented by Min et al. (1976). In their experiments on the transport of ethanol and water across a cellophane membrane, it was shown that under certain conditions it was possible to generate net mass transfer of ethanol against its concentration gradient. The membrane wedge interferometer experimental system used by Min et al. (1976) involved no temperature or hydrostatic pressure driven flows, and the countergradient transport results for ethanol were ascribed to diffusional coupling effects due to the greater transport of water through the cellophane membrane.

In the present paper we delineate further experimental studies of countergradient transport in the ethanol-water-

Correspondence concerning this paper should be addressed to R. H. Notter, Department of Radiation Biology and Biophysics, University of Rochester, School of Medicine and Dentistry, Rochester, New York 14642.

cellophane membrane system. In particular, the membrane wedge interferometer is used to determine transmembrane mass fluxes of ethanol and water over a binary solution concentration range that is sufficient to define the extent and characteristics of the countergradient transport regime. These experiments are then supplemented with a continuum theory analysis of a related but idealized membrane transport system to permit further description of the countergradient mass transfer process.

CONCLUSIONS AND SIGNIFICANCE

Membrane wedge interferometer experiments on the water-ethanol binary show net countergradient mass transfer of ethanol through a cellophane membrane over a wide range of ethanol concentration. In addition, similar countergradient mass transfer results and characteristics are predicted by a continuum theory analysis. These experimental and theoretical results thus confirm and extend the earlier data of Min et al. (1976) on a similar system and clearly show that in certain membrane transport situations, countergradient transport of a specific component can be generated solely by diffusional coupling effects. The diffusional transport in the experiments here is generated only by concentration differences of ethanol and water across the cellophane membrane separating two binary bulk solutions. A nonzero system mass average velocity results from differences in the mass transfer barrier presented by the membrane to the diffusing species. This diffusion generated mass average velocity is directed along the gradient of the most permeable component (water). Net countergradient flow of the less permeable species (ethanol) results when enough of this component is carried by the system mass average velocity to outweigh diffusive transport down its concentration gradient in the opposite direction.

A primary area of relevance for the experimental and theoretical results found here concerns the phenomenon of solvent drag which is present in many biological systems. For example, solvent drag effects have been found in a number of transport systems in the mammalian kidneys and intestines, where such transport typically involves the movement of various solutes during water absorption. The theoretical and experimental results here reinforce the necessity of accounting for coupled diffusion effects in the possible generation of countergradient transport before more complicated active transport explanations are invoked.

The phenomenon of countergradient mass transfer is of basic import in many physiological and bioengineering processes. This phenomenon has been documented by experimental studies in a wide variety of biological systems, and during the past two decades there has been significant interest in the development of a thorough understanding and characterization of countergradient transport. A majority of the relevant experimental and theoretical studies have been concerned with so called active transport systems, where the countergradient transport is achieved by the net expenditure of energy which may be furnished to the system, for example, by a chemical reaction. Although active countergradient transport is of primary significance in many physiological organ systems such as the mammalian kidney and intestines, the net transport of a specific substance against its concentration gradient does not necessarily mean that active processes requiring energy input to the system are involved. One important example of such transport involves diffusive coupling in membrane transport systems where the membrane has different permeabilities and/or solubilities to the various diffusing species.

Coupled diffusion phenomena, often classed under the heading of solvent drag in the bioengineering and biological literature, have received increasing attention since the early work of Ussing (1952), Anderson and Ussing (1957), and Rosenberg and Wilbrandt (1957), among others, in the 1950's. Such phenomena are, in fact, now given mention along with active transport in the widely used medical physiology textbook edited by Ruch and Patton (1965). Examples of more recent experimental studies of solvent drag effects include Froemter et al. (1973) concerning kidney tubule transport and a series of papers by Ochsenfahrt and Winne (1973, 1974*a*, *b*) on intestinal transport. Theoretical considerations have also been addressed by a number of authors including Stender et al. (1973), Galev and Van Bruggen (1970), and Patlak and Rapoport (1971).

In spite of the interest in characterizing coupled diffusion phenomena in biological systems, several factors have proved detrimental to a comprehensive unambiguous description. In terms of experimental studies, the complex problems of characterizing biological diffusion systems in terms of such basic parameters as homogeneity and geometry have often precluded the unambiguous interpretation of data. Moreover, the complex interplay of diffusive, convective, and osmotic phenomena present in many membrane systems makes it difficult to assess the role and importance of transport interactions between the diffusing species.

In the present paper we characterize diffusive coupling effects in the transport of binary solutions through a membrane by both experimental and theoretical means. The experimental technique used here involves a recently reported membrane wedge interferometer apparatus that allows internal consistency checks on the one-dimensional steady state nature of the mass transfer and on the calculated mass fluxes through the membrane (Min, 1975; Min et al., 1975, 1976). Following the experimental results, a continuum theory analysis is applied to a related but idealized membrane transport system to display further details of the countergradient mass transfer process and to permit at least qualitative comparison with experiment.

EXPERIMENTAL MATERIALS AND METHODS

Materials

The membrane used in this study was a commercial cellophane dialyzer membrane (#70158-1, Central Scientific Company, Chicago, Illinois). The membrane was washed repeatedly in ethanol and distilled water to remove any soluble impurities prior to use in actual transport experiments. Binary

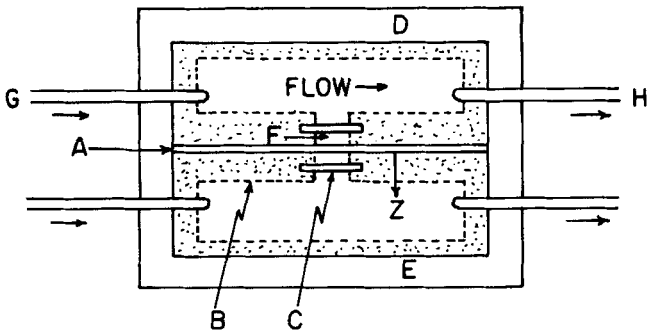

Fig. 1. Flow system for membrane wedge experiment: A. membrane; B. silastic rubber spacer; C. agar barrier; D. optical wedge I; E. optical wedge II; F. closed well region; G. inlet tube, wedge I; H. outlet tube, wedge I.

solutions were made from 200 proof ethyl alcohol (Publicker Industries, Linfield, Pennsylvania) and triply distilled water. All experiments were carried out at room temperature, 25 ± 2°C.

Methods

The experimental method used to characterize the one-dimensional, steady state fluxes of ethanol and water through cellophane was the membrane wedge interferometer. The details of this method are described elsewhere (Min, 1975; Min et al., 1976), and only a summary is given here. The apparatus consists essentially of two identical optical wedges set side by side and separated by a membrane. Each optical wedge is formed by separating optically flat (¼ wavelength of helium-neon laser light) partially metallized glass plates with silastic spacers. As shown in Figure 1, binary solutions of uniform but different concentration are made to flow through each optical wedge in a direction parallel to the membrane (A) separating optical wedges I and II (D and E in Figure 1). Mass transfer through the membrane from one wedge to the other is then initiated by the concentration difference between these binary bulk solutions. The flow of the solutions parallel to the membrane is driven by gravity from raised reservoirs, and the heights of these reservoirs are maintained so that bulk pressure is equalized between the two flowing solutions at any position.

In the membrane wedge interferometer experimental design, any convection effects from the bulk solutions flowing parallel to the membrane are made negligible by the inclusion of semi-transparent agar gel barriers, apparent as C on Figure 1. Thus, the regions that are characterized in terms of diffusional transport from one binary bulk solution to another through the cellophane membrane separating the two phases are the closed well regions (F) shown in Figure 1. Because of the presence of the agar barriers at the outer boundary of each closed well, these closed well regions are influenced solely by diffusion through the membrane, with the flowing solutions outside the barriers acting as a source or sink of new material necessary to achieve steady state, one-dimensional transport normal to the membrane in each closed well.

In the wedge membrane technique, the concentration field in each closed well is found from photographed interference patterns. These interference patterns are generated by means of helium-neon laser light transmitted from top to bottom through each wedge. The shape of these interference patterns is directly dependent on the refractive index field present in a given wedge, as discussed in detail elsewhere (Min, 1975; Min et al., 1975, 1976). Thus, the interference patterns generated from the wedge membrane apparatus represent a direct measure of the refractive index field present in the closed wells of the two optical wedges. Since the dependence of refractive index on concentration is well known for the ethanol-water binary (*International Critical Tables*, Vol. VII, 1930), the concentration field in the binary bulk phases surrounding the membrane can thus be determined.

Once the concentration fields in the closed well regions of Figure 1 are known, the mass fluxes of ethanol (n_A) and water (n_B) through the membrane can be calculated by equations given by Min et al. (1976). The method described there allows both n_A and n_B to be determined from concentration field data on only one side of the cellophane membrane, thus allowing data from the second closed well to be used as an internal consistency check on the n_A and n_B flux values. Moreover, the flux calculation method (Min et al., 1976) also allows a direct check on the one dimensionality of the diffusion through the membrane and on the steady state nature of the concentration field.

Table 1. Ethanol (A) and Water (B) Mass Fluxes Through a Cellophane Membrane at 25°C (Tam, 1976)

Run No.	Mass fraction of A in flowing bulk solutions*	Membrane thickness ($2l$) $\times 10^2$ cm	n_A $\times 10^6$ g/cm²-s	n_B $\times 10^5$ g/cm²-s
1	Wedge I = 0.30 II = 0.0	0.373	+3.00	−1.63†
2	0.30 0.05	0.362	+1.04	−1.45
3	0.30 0.10	0.354	−.55	−1.95
4	0.30 0.20	0.334	−.91	−1.00
5	0.30 0.40	0.314	+2.38	+1.03
6	0.20 0.0	0.380	+2.85	−1.70
7	0.20 0.5	0.369	+.82	−1.85
8	0.40 0.0	0.370	+3.26	−1.25
9	0.40 0.05	0.358	+1.14	−1.57
10	0.40 0.10	0.348	−.29	−1.71

* See Figure 1 for orientation.

† It is noted that the n_A and n_B values reported here for runs 1 to 3 and 6 to 7 differ from those reported by Min et al. (1976) for similar experimental conditions by an average absolute magnitude of 33% for the n_A values and 12% for the n_B values, apparently because of variabilities in digitalizing interferogram photographs (Tam, 1976). In all these comparable cases, however, the major features of the transport results are identical between the two studies in terms of whether or not countergradient transport was present.

EXPERIMENTAL RESULTS AND DISCUSSION

In the following presentation of experimental results, ethanol is designated as component A and water as component B. The component mass flux results for a series of ten experiments on the ethanol-water-cellophane membrane system are shown in Table 1. Further details such as extrapolated membrane solution boundary concentrations for these experiments are given by Tam (1976). In Table 1, the sign associated with a given mass flux value n_A or n_B refers to its direction relative to the z coordinate of Figure 1, where a positive sign indicates a direction of transport from wedge I to wedge II. *Each* n_A or n_B value in Table 1 represents an arithmetic average of fluxes calculated from concentration field data on the two sides of the membrane. In terms of internal consistency, an average deviation of ±11% about these mean values was found between n_A and n_B values calculated from data on a single side of the membrane for the ten experiments.

In terms of the magnitudes of the experimental mass flux measurements, it is clear from Table 1 that cellophane

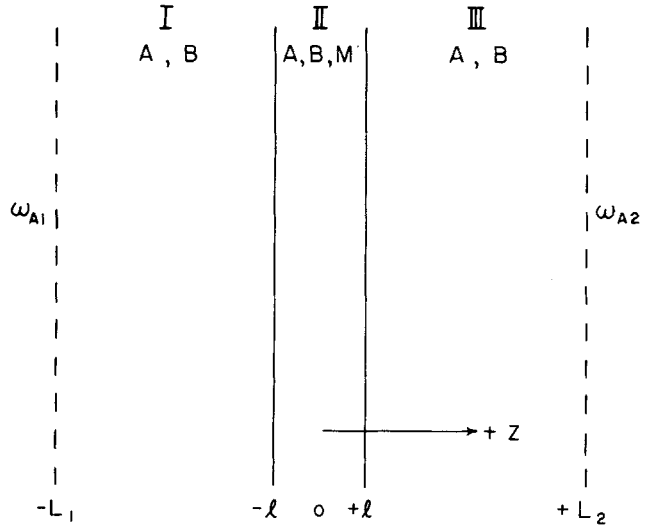

Fig. 2. Coordinate system for membrane transport analysis.

is far more permeable to water than it is to ethanol. In particular, the total mass flux of water relative to membrane fixed coordinates (n_B) is about an order of magnitude greater than the corresponding mass flux of ethanol (n_A). This mass flux difference for the two diffusing species requires a nonzero mass average velocity for the diffusion system; that is, the total system mass flux $n = n_A + n_B$ is nonzero. This diffusion generated system mass average velocity carries with it some ethanol, and for experimental runs 3, 4, 5, and 10, the amount of ethanol carried with the system mass average velocity was larger than the diffusive transport of ethanol down its concentration gradient in the opposite direction. Thus, for these four experiments, the net mass transfer of ethanol is against its concentration gradient; that is, diffusive coupling effects were large enough to generate countergradient transport. This is shown by the data of Table 1, where the algebraic signs of the ethanol and water mass fluxes are the same for experimental runs 3, 4, 5, and 10. For example, in run 3, the negative sign for $n_A = -0.55 \times 10^{-6}$ g/cm^2-s indicates that ethanol is undergoing a net mass flux from wedge II to wedge I, which is the same direction indicated by the corresponding water mass flux of $n_B = -1.95 \times 10^{-5}$ g/cm^2-s. However, the overall concentration driving force for ethanol diffusion is in the opposite direction, since the bulk mass fraction concentration of ethanol in wedge I is 0.3, while in wedge II it is only 0.1.

The data of Table 1 thus clearly display that countergradient transport through a membrane can be generated in a diffusion system driven solely by concentration gradient effects. The data also show that such transport will not occur under all circumstances, but only if sufficient amounts of the given component (A, ethanol in this case) are available to be carried by the system mass average velocity. For example, in run 2, countergradient transport of ethanol from wedge II to wedge I does not occur, even though the wedge I to wedge II concentration difference is quite similar to that present in run 3. The reason for this is that in run 2, the ethanol carried from wedge II by the system mass average velocity is present only in a mass fraction of 0.05, while in run 3 the corresponding ethanol concentration in wedge II is 0.10. This and other salient features of the transport results are made clearer in the theoretical analysis below.

THEORETICAL DEVELOPMENT

The presence of a membrane in a diffusion system adds several complexities to a transport analysis. Bulk diffusion in the phases separated by the membrane is still important, but there are added processes of dissolution into or out of the membrane as well as diffusion through the membrane to be described.

There are, in principle, several approaches that can be used to relate mass fluxes to the relevant driving forces. For example, the techniques of irreversible thermodynamics are often used to describe mass flux-driving force relationships in membrane transport systems (Ginzburg et al., 1963; Kaufman and Leonard, 1968; Kedem and Katchalsky, 1958; Kirkwood, 1954; Staverman, 1952). In the present paper, a phenomenological approach based on Fick's law is chosen to describe the mass transfer process. This approach has been verified in terms of accuracy and utility for the description of a wide variety of mass transfer phenomena in various engineering and biological systems (Bird et al., 1960; Lightfoot, 1974).

The theoretical model to be analyzed here is an ideal system of mass transfer across an infinite membrane separating two binary bulk solutions, as shown in Figure 2. The two nonionic bulk solution components are designated by A and B, and the membrane material is assumed to be homogeneous and denoted as component M. The membrane surfaces are defined by positions $z = \pm l$. Very far from the membrane surfaces, at positions $z = -L_1$ and $z = L_2$, the bulk phase concentrations are fixed at mass fraction $\omega_A = \omega_{A1}$ and $\omega_A = \omega_{A2}$, respectively. If ω_{A1} and ω_{A2} are different in magnitude, and if the temperature and pressure on both sides of the membrane are fixed and equal, then mass transfer through the membrane will be initiated by the $\omega_{A1} - \omega_{A2}$ concentration difference. The equations describing the mass concentrations and mass fluxes of components A and B at steady state can then be developed.*

In this theoretical analysis, the membrane is assumed to be fixed in space so that the velocity of the membrane itself is zero; that is, membrane fixed coordinates are employed. In general, the total mass flux (n_i) of a given system component i may be written as the sum of two contributions: a diffusive mass flux and a convective mass flux due to the overall system mass average velocity. For the present analysis as defined in Figure 2, all of the mass transfer phenomena are taken as one dimensional in direction z normal to the membrane. The system is at a constant temperature and bulk pressure, and the relevant mass flux of component A in the binary bulk solution regions I and III of Figure 2 is given by (for example, Bird, 1960)

$$n_A{}^I = -\rho^I \mathcal{D}_{AB}{}^I \frac{d\omega_A{}^I}{dz} + \omega_A{}^I(n_A{}^I + n_B{}^I) \qquad (1)$$

and

$$n_A{}^{III} = -\rho^{III} \mathcal{D}_{AB}{}^{III} \frac{d\omega_A{}^{III}}{dz} + \omega_A{}^{III}(n_A{}^{III} + n_B{}^{III}) \qquad (2)$$

In the membrane itself, region II in Figure 2, the situation is more complicated than in the binary bulk solutions regions I and III. Specifically, even if the membrane material is assumed homogeneous and denoted as component M, region II is still composed of a ternary mixture of A, B, and M. For the present idealized analysis, a so-called pseudo binary assumption (for example, Light-

* It is noted that the geometry of the theoretical model shown in Figure 2 is not precisely equivalent to the geometry of the experimental system of Figure 1, since the agar barriers themselves constitute an additional outer region on each side of the cellophane membrane. However, the addition of two more outer regions to the theoretical model can be shown to add no new conceptual features to the transport analysis (Tam, 1976).

foot, 1974) is used to describe the mass transfer in the membrane. Essentially, this assumption implies that the diffusion of A in the ternary system $(A + B + M)$ can be approximated by the diffusion of A in a binary system, where the second component is taken to be $B + M$. Similarly, the diffusion of B in the ternary system is described as the diffusion of B in a binary system, with the second component taken as $A + M$. With this assumption, the mass fluxes of A and B in the membrane region II are given by

$$n_A^{II} = -\rho^{II}\,\mathcal{D}_A^{II}\frac{d\omega_A^{II}}{dz} + \omega_A^{II}(n_A^{II} + n_B^{II} + n_M^{II}) \quad (3)$$

and

$$n_B^{II} = -\rho^{II}\,\mathcal{D}_B^{II}\frac{d\omega_B^{II}}{dz} + \omega_B^{II}(n_A^{II} + n_B^{II} + n_M^{II}) \quad (4)$$

It should be stressed that the pseudo binary diffusion coefficients $\mathcal{D}_A^{II}$ and $\mathcal{D}_B^{II}$ in Equations (3) and (4) are macroscopic parameters. In effect, they give a measure of the overall diffusive resistance presented by the membrane to the transporting species A and B. On the molecular level, such diffusive resistance is, of course, due to a combination of complex phenomena involving intermolecular forces and collisional interactions between A, B, and M. All of these complex effects are lumped together and expressed in terms of effective pseudo binary diffusion coefficients $\mathcal{D}_A^{II}$ and $\mathcal{D}_B^{II}$. This kind of approximate but useful description has been followed in the biological and bioengineering literature for systems ranging from bilayer lipid membranes (BLM) of the order of 10^2 Å thick to dialysis membranes of the order of 10^5 to 10^6 Å thick (Lightfoot, 1974) and thus has rather general relevance.

Equations (1) to (4) are the basic relations for the mass fluxes of A and B through the membrane M. These equations are subject to various constraints and boundary conditions as follows:

Constraints on Equations (1) to (4)

$$n_M = 0 \quad \text{(membrane fixed coordinates)} \quad (5)$$

$$\omega_A^I + \omega_B^I = 1 \quad (6)$$

$$\omega_A^{II} + \omega_B^{II} + \omega_M^{II} = 1 \quad (7)$$

$$\omega_A^{III} + \omega_B^{III} = 1 \quad (8)$$

Boundary Conditions on Equations (1) to (4)

$$\omega_A^I = \omega_{A1} \quad \text{at } z = -L_1 \quad (9)$$

$$\omega_A^{III} = \omega_{A2} \quad \text{at } z = L_2 \quad (10)$$

$$\omega_A^{II} = k_A\omega_A^I \quad \text{at } z = -l$$

$$\omega_B^{II} = k_B\omega_B^I = k_B(1 - \omega_A^I) \quad \text{at } z = -l \quad (11)$$

$$\omega_A^{II} = k_A\omega_A^{III} \quad \text{at } z = +l$$

$$\omega_B^{II} = k_B(1 - \omega_A^{III}) \quad \text{at } z = +l \quad (12)$$

The first two boundary conditions, Equations (9) and (10), are statements of the fact that far from the membrane surface, the bulk phase compositions are fixed at constant values ω_{A1} and ω_{A2}. Also, Equations (11) and (12) express the assumption of equilibrium at the membrane-solution interface, so that the concentrations in the membrane at the interface are given by a distribution coefficient k_A or k_B times the respective bulk solution concentrations at the interface. Thus, all solubility effects at the membrane-solution interface are lumped together and expressed in terms of a single macroscopic solubility parameter, the distribution coefficient.

Before we solve Equations (1) to (4), subject to the above constraints and boundary conditions, several additional simplifications may be imposed. In the membrane wedge experiments discussed earlier, steady state mass transfer was achieved. For the case of steady state mass transfer in the constant cross-sectional area theoretical model used here, it is necessary that the fluxes of A and B be constant and uniform in all three regions; that is

$$n_A^I = n_A^{II} = n_A^{III} = n_A \quad (13)$$

and

$$n_B^I = n_B^{II} = n_B^{III} = n_B \quad (14)$$

where n_A and n_B are now constants with position z. Furthermore, at steady state, there is the added requirement that the total flux with respect to fixed coordinates is constant; that is

$$n_A + n_B = K \quad (15)$$

In addition to the steady state restrictions, it will also be assumed that the product of overall density and diffusivity is constant in each of the three regions of the model;* that is

$$\rho^I\,\mathcal{D}_{AB}{}^I = \rho^{III}\,\mathcal{D}_{AB}{}^{III} = \mathcal{D} \quad (16)$$

$$\rho^{II}\,\mathcal{D}_A{}^{II} = D_A \quad (17)$$

$$\rho^{II} = \mathcal{D}_B{}^{II} = D_B \quad (18)$$

where $\mathcal{D}$, D_A, and D_B are constants.

In summary, the general membrane transport model to be solved is defined at steady state by the differential Equations (1) to (4) subject to the boundary conditions (9) to (12) and the additional requirements and assumptions of (13) to (18). The four first-order ordinary differential equations may be solved for $K \neq 0$, and the boundary conditions (9) to (12) applied to give (Tam, 1976)

$$\omega_A^I = \frac{n_A}{K} + \left(\omega_{A1} - \frac{n_A}{K}\right)e^{\frac{K}{\mathcal{D}}(z + L_1)} \quad (19)$$

$$\omega_A^{II} = \frac{n_A}{K} + \left[\frac{n_A}{K}(k_A - 1) + k_A\left(\omega_{A1} - \frac{n_A}{K}\right)e^{\frac{K}{\mathcal{D}}(L_1 - l)}\right]e^{\frac{K}{D_A}(z + l)} \quad (20)$$

$$\omega_B^{II} = \frac{n_B}{K} + \left[\frac{n_B}{K}(k_B - 1) - k_B\left(\omega_{A1} - \frac{n_A}{K}\right)e^{\frac{K}{\mathcal{D}}(L_1 - l)}\right]e^{\frac{K}{D_B}(z + l)} \quad (21)$$

$$\omega_A^{III} = \frac{n_A}{K} + \left(\omega_{A2} - \frac{n_A}{K}\right)e^{\frac{K}{\mathcal{D}}(z - L_2)} \quad (22)$$

In Equations (19) to (22), the unknowns left to be determined are the fluxes n_A and n_B or, equivalently, n_A and $K = n_A + n_B$. These unknowns are found by applying boundary condition (12) at $z = +l$ to Equations (20) and (22) and to Equations (21) and (22). The

* This assumption is more reasonable in many liquid phase diffusion systems than the assumption that overall density and diffusivity are independent of concentration individuality; it is, however, not exact for the experimental ethanol-water-cellophane membrane system.

result is two equations for the two unknowns n_A and K in the form

$$\frac{n_A}{K} = \frac{\omega_{A1}\, e^{\left[\frac{K}{\mathcal{D}}(L_1 - l) + \frac{2Kl}{D_A}\right]} - \omega_{A2}\, e^{\frac{K}{\mathcal{D}}(l - L_2)}}{\left\{\left(1 - \frac{1}{k_A}\right)\left[1 - e^{\frac{2Kl}{D_A}}\right] + e^{\left[\frac{K}{\mathcal{D}}(L_1 - l) + \frac{2Kl}{D_A}\right]} - e^{\frac{K}{\mathcal{D}}(l - L_2)}\right\}} \tag{23}$$

and

$$\frac{n_A}{K} = \frac{\left\{\left(1 - \frac{1}{k_B}\right)\left[1 - e^{\frac{2Kl}{D_B}}\right] + \omega_{A1}\, e^{\left[\frac{K}{\mathcal{D}}(L_1 - l) + \frac{2Kl}{D_B}\right]} - \omega_{A2}\, e^{\frac{K}{\mathcal{D}}(l - L_2)}\right\}}{\left\{\left(1 - \frac{1}{k_B}\right)\left[1 - e^{\frac{2Kl}{D_B}}\right] + e^{\left[\frac{K}{\mathcal{D}}(L_1 - l) + \frac{2Kl}{D_B}\right]} - e^{\frac{K}{\mathcal{D}}(l - L_2)}\right\}} \tag{24}$$

Unfortunately, Equations (23) and (24) are transcendental in the total flux $K = n_A + n_B$, and so it is not possible to solve algebraically for the fluxes n_A and n_B. It is possible, however, to solve these equations numerically for n_A and n_B to display the conditions under which countergradient transport of one of the species A or B will occur owing to direct diffusional coupling with the other component. Such numerical solutions have been carried out here and are presented later.

It is noted that the flux relations in Equations (23) and (24) are for the case of total flux $K = n_A + n_B \neq 0$. The special case where $K = 0$ can be solved explicitly for the fluxes. If Equations (1) to (4) are written for $K = 0$, solution with the boundary conditions and assumptions given above for the general case yields (Tam, 1976)

$$n_A = -n_B = \frac{k_A(\omega_{A1} - \omega_{A2})}{k_A(L_1 + L_2 - 2l)/\mathcal{D} + 2l/D_A} \tag{25}$$

subject to the constraint

$$\frac{k_A D_A}{k_B D_B} = 1 \quad \text{for} \quad K = 0 \tag{26}$$

The constraint expressed by Equation (26) is required by the fact that in order for the fluxes of A and B to be equal and opposite, the membrane must present the same overall barrier to each species. This barrier is composed of two effects in Equation (26): a solubility effect expressed in terms of distribution coefficients k_A and k_B and a diffusion effect represented by effective diffusion coefficients D_A and D_B.

THEORETICAL RESULTS AND DISCUSSION

The theoretical flux results given in Equations (23) and (24) contain many parameters, including boundary concentrations (ω_{A1}, ω_{A2}), distribution (solubility) coefficients (k_A, k_B), density-diffusivity products ($\mathcal{D}$, D_A, D_B), and length parameters (l, L_1, L_2). A complete parametric study where all of the above quantities would be varied independently was not attempted. Instead, numerical solutions were found for most of these parameters fixed at values relevant for the experimental ethanol-water-cellophane membrane system discussed previously.

The length values chosen were $l = 0.002$ and $L_1 = L_2 = 0.2$ cm. These values correspond closely to the geometry of the membrane wedge interferometer closed well regions of Figure 1 and to the thickness of the cellophane membrane studied (Tam, 1976). The distribution coefficients k_A and k_B were both fixed equal to 0.4, although this may be in error by as much as 50% for ethanol in cellophane as discussed by Tam (1976). However, precise values for ethanol and water distribution coefficients in cellophane are not available, and in any case, even extreme changes in distribution coefficient do not negate the countergradient transport conclusions ultimately drawn from the numerical solutions. Thus, for simplicity, the distribution coefficients for A and B were fixed equal at 0.4 in all calculations. Also, the value of $\mathcal{D}$, the bulk phase density-diffusivity product [Equation (16)] was fixed at 10^{-5} g/cm-s, close to the relevant values for the ethanol-water binary at 25°C.

In the final numerical calculations, two sets of parameters (D_B/D_A) and (ω_{A1}, ω_{A2}) were varied to investigate the trends in the fluxes n_A and n_B. Equations (23) and (24) were combined into a single nonlinear equation of the form $f(K) = 0$. This equation was then solved by a Newton-Raphson iteration technique on an IBM 370/168 computer.* The resultant solutions are plotted in terms of n_A or n_B as a function of ω_{A2} at fixed $\omega_{A1} = 0.3$ or $\omega_{A1} = 0.0$ on Figures 3 to 6. Each graph is a family of n_A or n_B curves at various D_B/D_A ratios, with D_A fixed at 10^{-7} gm/cm-s. This fixed D_A value is approximately that found by Min (1975) for ethanol diffusion through cellophane and is chosen to facilitate later comparisons with experimental results.

The numerical solution results in Figures 3 and 4 show the fluxes n_A and n_B as functions of ω_{A2} for fixed $\omega_{A1} = 0.3$ (see Figure 2 for orientation). In the absence of any system mass average velocity (the case of $K = 0$), it would be expected that in the range $0 \leq \omega_{A2} < 0.3$, species A would diffuse in the $+z$ direction ($n_A > 0$) down its concentration gradient, while species B would diffuse with equal magnitude in the $-z$ direction ($n_B < 0$). Similarly, for $0.3 < \omega_{A2} \leq 1.0$, species A should diffuse in the $-z$ direction ($n_A < 0$), and species B should diffuse with equal magnitude in the $+z$ direction ($n_B > 0$). When $\omega_{A2} = 0.3$, there is no concentration gradient driving force, and both n_A and n_B should be equal to zero at this point. In general, any $K = 0$ case is represented on Figures 3 and 4 by the $D_B/D_A = 1$ line, since the numerical solutions are all found for the case $k_A = k_B$ [see Equation (26)]. Thus, the $D_A/D_B = 1$ line on Figures 3 and 4 represents simple equimolar counterdiffusion, with the fluxes of A and B directly proportional to the imposed concentration gradient driving force.

* For computer program details and tabulated numerical solutions values, see Tam (1976).

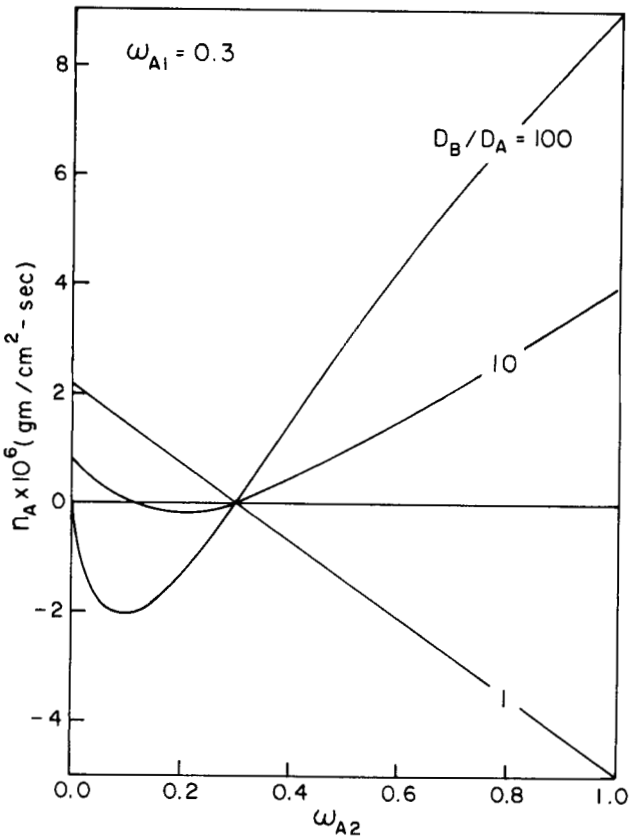

Fig. 3. Dependence of model flux of A on ω_{A2} at $\omega_{A1} = 0.3$.

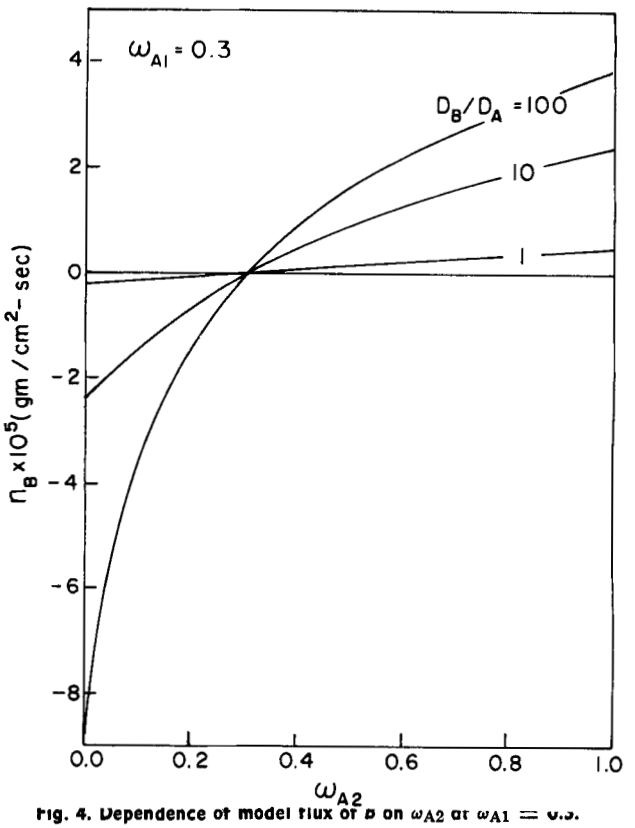

Fig. 4. Dependence of model flux of B on ω_{A2} at $\omega_{A1} = 0.3$.

As soon as D_B/D_A becomes greater than one, this means that the membrane is more permeable to species B than to species A, and hence the steady state fluxes n_A and n_B are no longer equal in magnitude. Thus, for $D_B/D_A > 1$, there is a net mass average velocity imposed on the system by the diffusion field, and diffusion generated convection effects are then superimposed on the diffusive transport. This fact does not affect the direction of net transport for the more permeable species B, since the greater B flux

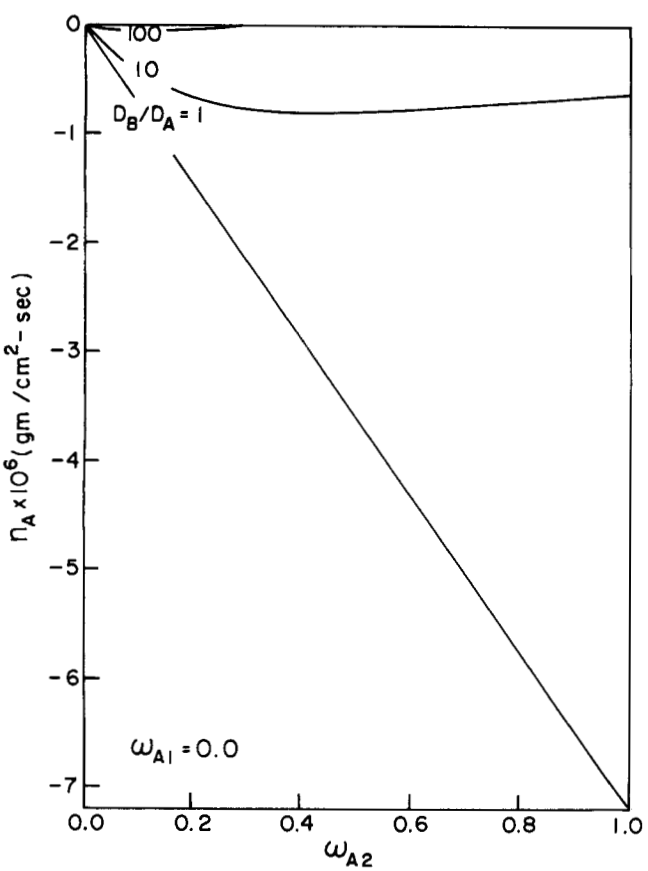

Fig. 5. Dependence of model flux of A on ω_{A2} at $\omega_{A1} = 0.0$.

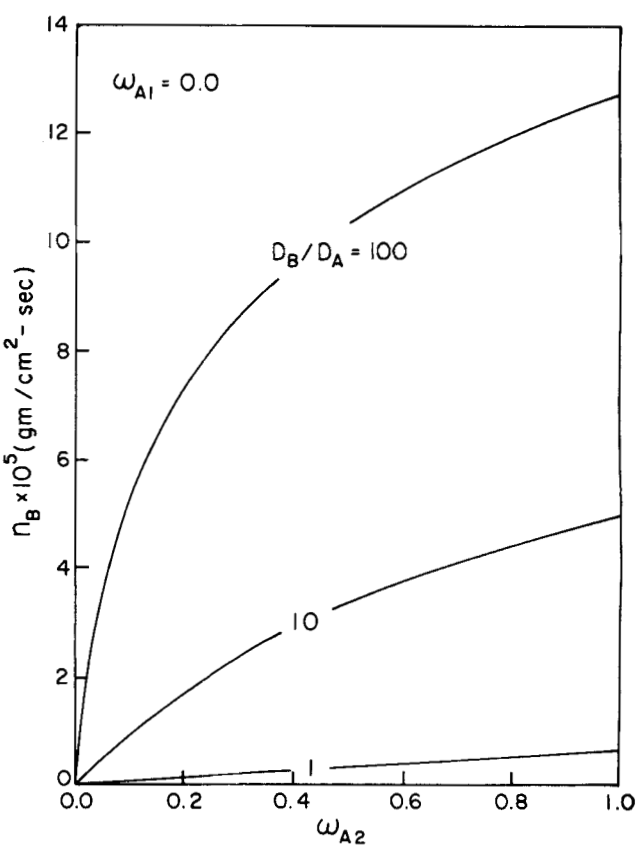

Fig. 6. Dependence of model flux of B on ω_{A2} at $\omega_{A1} = 0.0$.

is in effect generating the convection. It does, however, affect the direction of transport for the less permeable component A if enough of this component is carried by the nonzero mass average velocity to outweight diffusive transport in the opposite direction. This situation is shown clearly by the $D_B/D_A = 10$ and $D_B/D_A = 100$ curves on Figures 3 and 4. Specifically, the direction of net transport of B in Figure 4 is always in the direction of its concentration gradient; that is, with $\omega_{A1} = 0.3$, n_B is less than zero for $0 \leq \omega_{A2} < 0.3$, and n_B is greater than zero for $0.3 < \omega_{A2} \leq 1$. This is not true, however, for the mass flux of A shown in Figure 3. For example, for $D_B/D_A = 10$, the results in Figure 3 show $n_A < 0$ for ω_{A2} between approximately 0.1 and 0.3 and $n_A > 0$ for $\omega_{A2} > 0.3$. Thus, over this entire range, the direction of net total flux of species A is the same as the direction of net total flux for species B; that is, species A is undergoing net mass transfer against its concentration gradient. This effect is even more dramatic along the $D_B/D_A = 100$ curve of Figure 3, where species A undergoes net countergradient mass transport over the entire concentration range except for values of $\omega_{A2} \to 0$.

The reason that diffusional coupling effects cannot generate countergradient mass transport of A as $\omega_{A2} \to 0$ is as follows. For $\omega_{A1} = 0.3$ and $\omega_{A2} \to 0$, the diffusion of species B is directed in the $-z$ direction, and this is then the direction of the nonzero mass average velocity imposed by the diffusion of the more highly permeable component B. Thus, mass average velocity convection effects are present from $+z$ to $-z$ for the $\omega_{A2} \to 0$ case as long as $D_B/D_A > 1$. However, this convection at steady state can only carry along species A of initial concentration equal to ω_{A2}, the concentration of A present at the outer boundary at $z = +L_2$. Thus, as $\omega_{A2} \to 0$, no matter how large the mass average velocity due to the greater B permeability becomes, it does not have any species A to carry in order to generate countergradient mass transfer. Within the constraints of the model, the most convection can do as $\omega_{A2} \to 0$ is to swamp out the concentration gradient driven diffusion of A and thus cause n_A to approach zero. This occurs for the $D_B/D_A = 100$ curve on Figure 3, where $n_A \to 0$ as $\omega_{A2} \to 0$. For the $D_B/D_A = 10$ curve on the same figure, the smaller system mass average velocity is not sufficient to outweigh completely the concentration gradient driven diffusion of A, and n_A becomes nonzero and in the direction of its gradient as $\omega_{A2} \to 0$. However, for this $D_B/D_A = 10$ curve, there is a point ($\omega_{A2} \approx 0.1$) where the diffusion and convection of A just balance to give a total flux $n_A = 0$.

The reason for the minimums in the n_A vs. ω_{A2} curves of Figure 3 for $D_B/D_A > 1$ is directly related to the factors discussed above. As noted previously, all curves on this figure represent $\omega_{A1} = 0.3$. As ω_{A2} decreases from 0.3 for $D_B/D_A > 1$, mass average velocity convection effects from the greater B diffusion arise. These convection effects become greater as ω_{A2} decreases toward zero, corresponding to n_B values of increasing absolute magnitude. However, as $\omega_{A2} \to 0$, the larger resultant system mass average velocity actually has smaller coupling effects on the flux of A because there is less species A available to be carried by the system mass average velocity. These competing effects of greater system mass average velocity, but less A to be carried with it, cause the minimums observed in the $D_B/D_A > 1$ curves of Figure 3.

The theoretical considerations discussed in the context of Figures 3 and 4 are also applicable to the further theoretical results shown in Figures 5 and 6. Specifically, Figures 5 and 6 show n_A and n_B, respectively, vs. ω_{A2} for the case where ω_{A1} is fixed at zero. As discussed in detail above, when one of the boundary concentration values of A is fixed at zero, it is impossible to generate countergradient transport of A from coupling effects, regardless of the amount of convection generated by the greater B diffusion. This is clearly shown by Figures 5 and 6. The flux of B in Figure 6 is always in the direction of its concentration gradient and increases for a given driving force as D_B/D_A increases. However, the flux of A in Figure 5 is always directed opposite to that of B and approaches zero as D_B/D_A increases to the point where convection effects completely dominate.

The numerical solutions of Figures 3 and 4 clearly show extensive concentration ranges over which countergradient transport due to direct diffusive coupling can occur. Now we turn to a comparison of the theoretical results with the experimental data presented earlier.

COMPARISON OF EXPERIMENT AND THEORY

Although the idealized theoretical model just discussed displays several features of the countergradient transport process, a direct quantitative comparison of experimental and theoretical results is hindered by several factors. One difference between theory and experiment is that the theoretical solutions for n_A and n_B include the assumption that the density-diffusivity products ($\mathcal{D}$, D_A, D_B) are constants. This assumption, although not exact, was employed not only for mathematical simplicity but also because precise functional forms for the variation of the membrane coefficients D_A and D_B with the concentration are not known. However, to obtain the experimental mass flux values n_A and n_B in Table 1 from the membrane wedge interferometer, a knowledge of D_A and D_B is not required. Specifically, the only diffusion parameter that is required among the three above is the bulk phase density-diffusivity product $\mathcal{D}$ (Min et al., 1976; Tam, 1976). Since $\mathcal{D}$ values for the water-ethanol binary are well known as a function of concentration (Hammond and Stokes, 1953; Perry, 1950), concentration variations were taken into account in the calculations leading to the experimental n_A and n_B results in Table 1.

Another factor affecting comparison with theory concerns the lack of precise experimental values for the distribution coefficients of ethanol (k_A) and water (k_B) in cellophane. Because of this, exact values of the membrane diffusion coefficients D_A and D_B necessary for comparison with theory cannot be calculated from the experimental n_A and n_B values of Table 1. However, approximate values of k_A and k_B measured by Tam (1976) and Min (1975) suggest that D_A is of order 10^{-7} gm/cm-s while D_B is of order 10^{-6} gm/cm-s, leading to a D_B/D_A ratio of about 10.

With these differences between theory and experiment in mind, it is possible to put the experimental results of Table 1 into a form permitting at least qualitative comparison with theory. Specifically, the first five experiments of Table 1 were performed with one bulk solution fixed at $\omega_A = 0.3$ outside of the agar gel barrier. This bulk concentration may be identified as ω_{A1} if the closed well region and agar barrier (F and C, respectively, in Figure 1) of wedge I are lumped together as region I in the theoretical model.* Similarly, the bulk solution concentration in wedge II in experiments 1 to 5 may be identified as ω_{A2}. With these approximations, plots of experimental n_A and n_B values vs. ω_{A2} can be constructed at

* This approximation will be exact if the presence of the agar does not alter the binary diffusion characteristics of solutions of ethanol and water. Since the agar barriers used here were about 1% agar by weight, the approximation seems relatively good, especially for qualitative comparisons.

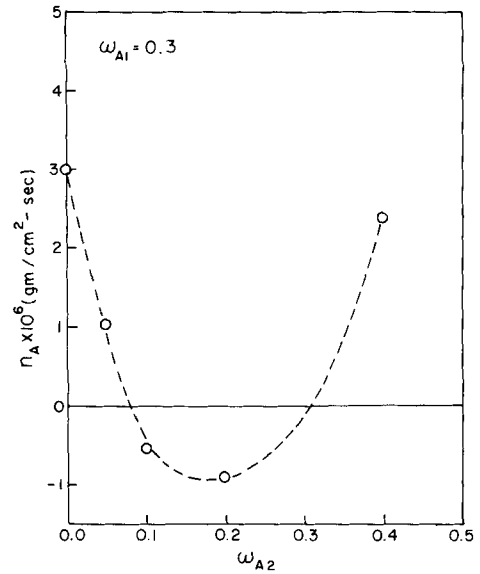

Fig. 7. Dependence of experimental flux of *A* on ω_{A2} at fixed $\omega_{A1} = 0.3$.

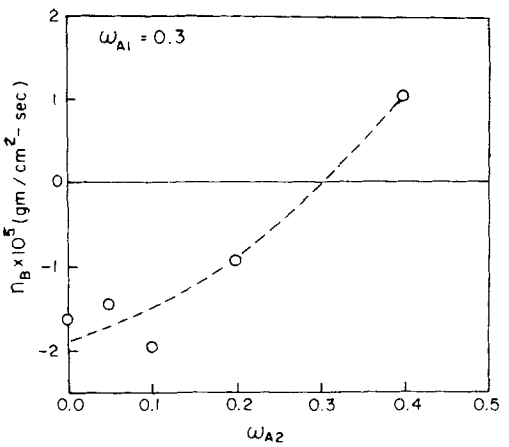

Fig. 8. Dependence of experimental flux of *B* on ω_{A2} at fixed $\omega_{A1} = 0.3$.

fixed $\omega_{A1} = 0.3$. Such plots are shown in Figures 7 and 8, and the results closely parallel the theoretical calculations of Figures 3 and 4.

As shown by Figures 3 and 7, both experimental and theoretical n_A values go through a minimum below $\omega_{A2} = 0.3$ and then become positive as ω_{A2} increases above 0.3. The experimental range of countergradient transport from Figure 7 is for $\omega_{A2} > \sim 0.08$, while the theoretical results of Figure 3 show a similar effect for $\omega_{A2} > \sim 0.1$ with $D_B/D_A = 10$. Similarly, the experimental n_B vs. ω_{A2} flux results of Figure 8 are always in the direction of the species *B* concentration gradient as is consistent with the model results of Figure 4. One difference in the theoretical and experimental n_B results is that the experimental n_B vs. ω_{A2} results of Figure 8 appear to be slightly concave upward, while the theoretical n_B results in Figure 4 are concave downward along a curve of constant $D_B/D_A = 10$. This difference is most likely due to the fact that D_B/D_A was not constant for the experimental flux values calculated for runs 1 to 5 but instead varied slightly from experiment to experiment because of concentration changes. Thus, the experimental points of Figure 8 do not really lie precisely along a constant $D_B/D_A = 10$ curve. In terms of the major features of the diffusion generated countergradient mass transport, however, the agreement between theory and experiment is clear.

In summary, then, both experimental and theoretical results clearly demonstrate that countergradient transport of a diffusing species through a membrane can be generated solely by diffusional coupling effects. The diffusional transport here is generated only by differences in the concentration of the transporting species across a membrane separating two bulk liquid phases. A nonzero system mass average velocity results from differences in the mass transfer barrier presented by the membrane to the diffusing components. This diffusion generated mass average velocity then leads to countergradient transport of the less permeable species if it is sufficient to outweigh passive diffusion effects.

In a simplistic fashion, diffusive mass transfer in biological systems takes place across two kinds of membranes: cell membranes and tissue membranes. Even though tissue membranes are composed essentially of cells, the second category is noted separately primarily because tissue membranes can support continuous net flow across themselves while cell membranes cannot. Since the countergradient transport analyzed here rests on the existence of a diffusion generated bulk flow, it is most relevant biologically in terms of transport across tissue membranes. In particular, such effects are most important in the kidney tubules and in the intestines, as indicated by the interest of many physiologists concerning solvent drag in these transport organs. Because of its small size and large physiologic concentration, water is by far the most important biological system component to act as the more permeable species *B* in the analysis here. In such systems where water transport is appreciable, there will typically be some transport of other chemical species by diffusional coupling effects. If the water flux is large compared to the flux of other system components, the results here show that these coupling effects can, in principle, be sufficient to generate countergradient transport over a wide range of concentrations. Moreover, even if the coupled diffusion effects are not sufficient to generate countergradient transport, the modifying influence of the resulting system mass average velocity should be included in transport data analysis and interpretation.

ACKNOWLEDGMENT

This paper is based on work performed partially under contract with the U.S. Department of Energy at the University of Rochester Department of Radiation Biology and Biophysics and has been assigned Report No. UR-3490-1463. The research was also supported in part by a Petroleum Research Fund Grant and by an NSF Institutional Grant. The authors would like to thank Professors J. L. Duda and A. D. Keith for their helpful comments and suggestions.

NOTATION

A, B = species *A*, species *B* in diffusion system (Figure 2)
$\mathcal{D}_{AB}$ = binary diffusion coefficient of *A*, *B*
$\mathcal{D}$ = $\rho\mathcal{D}_{AB}$, bulk phase density-diffusivity product
$\mathcal{D}_A^{II}$, $\mathcal{D}_B^{II}$ = effective diffusion coefficients of *A*, *B* in the membrane
D_A, D_B = $\rho^{II}\mathcal{D}_A^{II}$, $\rho^{II}\mathcal{D}_B^{II}$; membrane phase density-diffusivity products
k_A, k_B = distribution coefficients of *A*, *B* in membrane
K = total flux, $n_A + n_B$
l = one half of membrane thickness (Figure 2)
L_1, L_2 = positions of fixed bulk concentration far from membrane (Figure 2)
M = membrane material
n_i = mass flux of species i relative to membrane fixed coordinates (in z direction)
z = direction normal to membrane
ρ_i = density of species i

ρ = overall density $= \Sigma\rho_i$
ω_i = mass fraction of $i = \rho_i/\rho$
ω_{A1}, ω_{A2} = fixed mass fractions of A far from membrane (Figure 2)

Subscripts

A, B = species A, species B

Superscripts

I, III = bulk phase regions adjacent to membrane (Figure 2)
II = membrane region (Figure 2)

LITERATURE CITED

Anderson, B., and H. H. Ussing, "Solvent Drag on Non-Electrolytes During Osmotic Flow," *Acta Physiol. Scand.*, **39**, 228-239 (1957).

Bird, R. B., W. E. Stewart, and E. N. Lightfoot, *Transport Phenomena*, Wiley, New York (1960).

Froemter, E., G. Rumrich, and K. J. Ullrich, "Phenomenologic Description of Na^+, Cl^- and HCO_2 Absorption from Proximal Tubules of the Rat Kidney," *Pfluegers Arch. Eur. J. Physiol.*, **343**, 189-220 (1973).

Galey, W. R., and J. T. Van Bruggen, "The Coupling of Solute Fluxes in Membranes," *J. General Physiol.*, **55**, 220-242 (1970).

Ginzburg, B. Z., and A. Katchalsky, "The Frictional Coefficients of the Flow of Non-Electrolytes Through Artificial Membranes," *ibid.*, **47**, 403-418 (1963).

Hammond, B. R., and R. H. Stokes, "Diffusion in Binary Liquid Mixtures," *Trans. Faraday Soc.*, **49**, 890-895 (1953).

International Critical Tables, Vol. VII, p. 67, McGraw-Hill, New York (1930).

Kaufman, T. G., and E. F. Leonard, "Studies of Intramembrane Transport: A Phenomenological Approach," *AIChE J.*, **14**, 110-117 (1968).

Kedem, D., and A. Katchalsky, "Thermodynamic Analysis of the Permeability of Biological Membranes to Non-Electrolytes," *Biochimica et Biophysica Acta*, **27**, 229-246 (1958).

Kirkwood, J. G., "Transport of Ions Through Biological Membranes from the Standpoint of Irreversible Thermodynamics," in *Ion Transport Across Membranes*, H. T. Clarke and D. Nachmansohn, ed., Academic Press, New York (1954).

Lightfoot, E. N., Jr., *Transport Phenomena and Living Systems*, Wiley-Interscience, New York (1974).

Min, S., "Phenomenological Studies of Membrane Transport with a Wedge Interferometer," Ph.D. thesis, Pa. State Univ., University Park (1975).

———, J. L. Duda, and R. H. Notter, "Steady State Interferometric Studies of Membrane Transport," *Federation Proceedings Abstracts*, **34**, 325 (1975).

———, and J. S. Vrentas, "An Interferometric Technique for the Study of Steady State Membrane Transport," *AIChE J.*, **22**, 175-182 (1976).

Ochsenfahrt, H., and D. Winne, "The Contribution of Solvent Drag to the Intestinal Absorption of Tritiated Water and Urea from the Jejunum of the Rat," *Naunyn-Schmiedeberg's Arch. Pharmacol.*, **279**, 133-152 (1973).

———, "The Contribution of Solvent Drag to the Intestinal Absorption of the Basic Drugs Amidopyrine and Antipyrine from the Jejunum of the Rat," *ibid.*, **281**, 175-196 (1974*a*).

———, "The Contribution of Solvent Drag to the Intestinal Absorption of the Acidic Drugs Benzoic Acid and Salicylic Acid from the Jejunum of the Rat," *ibid.*, 197-217 (1974*b*).

Patlak. C. S., and S. I. Rapoport, "Theoretical Analysis of Net Tracer Flux Due to Volume Circulation in a Membrane with Pores of Different Sizes," *J. General Physiol.*, **57**, 113-124 (1971).

Perry, J. H., ed., *Chemical Engineering Handbook*, 3 ed., p. 188, McGraw-Hill, New York (1950).

Rosenberg, T., and W. Wilbrandt, "Uphill Transport Induced by Counterflow," *J. General Physiol.*, **41**, 289-296 (1957).

Ruch, T. E., and H. D. Patton, ed., *Physiology and Biophysics*, 19 ed., W. B. Saunders Co., Philadelphia, Pa. (1965).

Staverman, A. J., "Non-Equilibrium Thermodynamics of Membrane Processes," *Trans. Faraday Soc.*, **48**, 176-185 (1952).

Stender, S., K. Kristensen, and E. Skadhauge, "Solvent Drag by Solute-Linked Water Flow," *J. Membrane Biol.*, **11**, 377-398 (1973).

Tam, Y. M., "Characterization of Coupled Diffusion Effects with a Wedge Interferometer," M.S. thesis, Pa. State Univ., University Park (1976).

Ussing, H. H., "Some Aspects of the Application of Tracers in Permeability Studies," *Advances in Enzymology*, **13**, 21-65 (1952).

Manuscript received April 7, 1978; revision received October 30, and accepted January 11, 1979.

Fully Developed Viscous Flow and Heat Transfer in Curved Semicircular Sectors

The Navier-Stokes equation in stream function-vorticity form and the energy equation are solved numerically for a fully developed flow of a Newtonian fluid in coiled circular sectors having zero pitch. Two heat transfer cases are studied: axially uniform heat flux with uniform peripheral temperature and axially uniform temperature with mixed conditions along the periphery. Solutions are presented for curvature ratios in the range of 5 to 30, Prandtl numbers in the range of 0.7 to 100, and Dean numbers up to 300. In all cases studied, the heat transfer performance for the curved tubes was superior to that of a straight tube geometry.

JACOB H. MASLIYAH

Department of Chemical Engineering
University of Alberta
Edmonton, Alberta, Canada

and

K. NANDAKUMAR

Chemical Engineering Department
Princeton University
Princeton, New Jersey 08540

SCOPE

Curved tubes such as helical and spiral coils find a wide variety of application in heat exchangers and chemical reactors. The reason for such a wide use of coiled tubes are twofold. Coiled tubes make it possible to house process equipments such as heat exchangers in a very small space. More importantly, the existence of secondary flow in coiled tubes aids transfer processes such as convective heat and mass transfer.